

# PCCP

Accepted Manuscript



This is an *Accepted Manuscript*, which has been through the Royal Society of Chemistry peer review process and has been accepted for publication.

*Accepted Manuscripts* are published online shortly after acceptance, before technical editing, formatting and proof reading. Using this free service, authors can make their results available to the community, in citable form, before we publish the edited article. We will replace this *Accepted Manuscript* with the edited and formatted *Advance Article* as soon as it is available.

You can find more information about *Accepted Manuscripts* in the [Information for Authors](#).

Please note that technical editing may introduce minor changes to the text and/or graphics, which may alter content. The journal's standard [Terms & Conditions](#) and the [Ethical guidelines](#) still apply. In no event shall the Royal Society of Chemistry be held responsible for any errors or omissions in this *Accepted Manuscript* or any consequences arising from the use of any information it contains.

## Photo-induced dynamics of the heme centers in cytochrome $bc_1$

Cite this: DOI: 10.1039/x0xx00000x

Adrien A. P. Chauvet<sup>a</sup>, André Al Haddad<sup>a</sup>, Wei-Chun Kao<sup>b</sup>, Frank van Mourik<sup>a</sup>, Carola Hunte<sup>b</sup>, and Majed Chergui<sup>\*a</sup>

Received 00th January 2012,  
Accepted 00th January 2012

DOI: 10.1039/x0xx00000x

www.rsc.org/

The ultrafast response of cytochrome  $bc_1$  is investigated for the first time, via transient absorption spectroscopy. The distinct redox potentials both  $c_1$ - and  $b$ -hemes allows for a clear differentiation of their respective signals. We find that while the  $c_1$ -heme photo-product exhibits the characteristics of a 5-coordinated species, the  $b$ -hemes presumably undergo photo-oxidation at a remarkably high quantum yield. The  $c_1$ -heme iron-ligand recombination time is 5.4 ps, in agreement with previous reports on homologous cytochromes. The suggested photo-oxidized state of the  $b$ -hemes has a life-time of 6.8 ps. From this short life-time we infer that the electron acceptor must be within van der Waals contact with the heme, which points to the fact that the axial histidine residue is the electron acceptor. The different heme-responses illustrate the flexibility of the  $c_1$ -heme ligation in contrast to the more rigid  $b$ -heme binding, as well as the higher electronic reactivity of the  $b$ -hemes within the  $bc_1$  complex. This study also demonstrates the remarkable connection between the heme local environment and its dynamics and, therefore, biological function.

### Introduction

Cytochrome (cyt)  $bc_1$  complex is a key player in mitochondrial and bacterial respiratory chains.<sup>1</sup> It is the main actor in the protonmotive Q cycle as it catalyzes the two-electron oxidation of a quinol and the one-electron reduction of a  $c$ -type cytochrome and a quinone while conjugating this electron transfer to the formation of a proton gradient across the membrane.<sup>2-4</sup> The generated potential gradient serves as the driving force to the ATP synthesis, the universal energy transporter in living organisms.<sup>1</sup> Cyt  $bc_1$  complex is a dimer whose monomer comprises four key elements that are directly involved in the electronic pathway (Figure 1): (1) The heme  $c_1$  is located near the intermembrane-space side of the membrane; it is situated near the cyt  $c$  docking interface and serves as electron donor for the reduction of cyt  $c$ ;<sup>2, 5-7</sup> (2) The Rieske iron-sulfur cluster mediates electron transfer between the quinol at the  $Q_0$  site and the heme  $c_1$  via a series of conformational changes;<sup>1</sup> (3) and (4) The hemes  $b_L$  and  $b_H$  that mediate electron transfer between the two quinone binding sites,  $Q_0$  and  $Q_i$  sites.<sup>2</sup> Depending on the reaction stage, the three iron center of the hemes are found in either their ferric (Fe(III)) or ferrous forms (Fe(II)) and are all characterized by a 6-coordinated (6-c) low-spin state, therefore minimizing the reorganization energy required to undergo the electron transfer.<sup>8</sup>

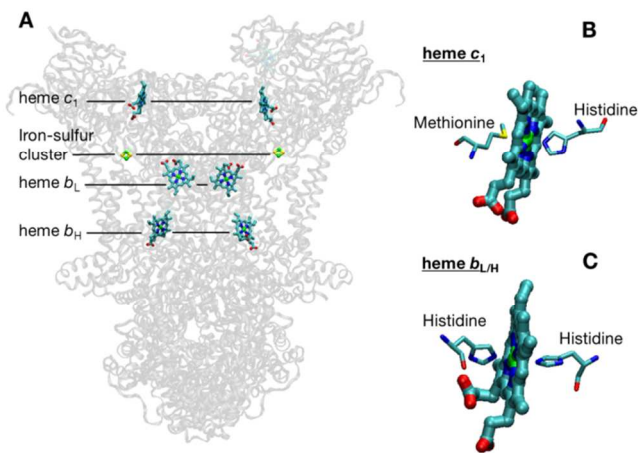


Figure 1: (A) Structure of the  $bc_1$  complex 7 with the protein backbone being shaded for clear visualization of the key actors in the proton-coupled-electron mechanisms. Structure of the heme- $c_1$  (B) and of the heme- $b$  (C) with their axial amino acid ligands.

Crystallographic data reveals that the  $c_1$ -heme is covalently attached via the vinyl groups to two cysteine residues and has both methionine (Met) and histidine (His) residues as axial ligands (Figure 1). The  $b$ -hemes however are not covalently attached to polypeptide and have two His residues as axial ligands.<sup>9</sup> Such differences in the structural environment confer to each heme-type their particular redox properties and specific

functions.<sup>10</sup> The origins of the overall catalytic functions of the  $bc_1$  complex remain however unknown. In this view, ultrafast spectroscopy is able to give access to the early mechanisms and local structural and electronic modifications that confer the heme-protein its overall functions. The ultrafast behaviors, and more specifically, the relaxation of photo-excited hemes, has indeed been the object of intense study since the late 1980s.<sup>11,12</sup> For example, the hemes in cyt *c* and cyt  $b_5$ , which are structurally comparable to the  $c_1$ - and *b*-hemes of the  $bc_1$  complex, respectively,<sup>13,14</sup> are known to dissociate from their axial ligand within femtoseconds as a response to light absorption.<sup>14-16</sup> While the early steps of the heme photo-cycle still raises questions, it is generally accepted that photo-excitation of the heme is followed by an electron transfer (ET) to the iron d-orbitals,<sup>16</sup> which in turn is believed to trigger the ligand dissociation in ferrous complexes. This photo-dissociation seems to be a universal feature in cyt's<sup>17</sup> but its relation to the overall functionality of the protein is unclear. There is no previous study of the cyt  $bc_1$  complex in the femto-picosecond regime, most probably due to the quantity and purity of sample required for such measurements. We therefore aim to complete our knowledge by presenting the first such study here. By means of ultrafast transient pump-probe spectroscopy, we bring to light the short-lived local electronic and nuclear modifications that are behind physiological processes and confer to the  $bc_1$  complex its overall functionalities.

Most works on cyt's focus on the Soret band region (~430 nm) for both, excitation and detection, as it is the most intense absorption band. In this work we focus on the weaker  $\alpha$ -band around 550-570 nm. The pump is tuned at 523 nm in order to indifferently excite via the  $\beta$ -bands both heme-types while in their ferrous states (see Figure 1). The reason for probing the  $\alpha$ -bands rather than the Soret band is that in the presence of multiple heme-types, the Soret band region in the  $bc_1$  complex is spectrally congested, while the  $\alpha$ -band region allows a clear distinction between the *b*- and *c*-hemes.<sup>18</sup> Furthermore, the  $\alpha$ -bands are sensitive to changes in the electronic states and coordination of the hemes.<sup>19</sup> Besides being spectrally distinguishable, each heme type has a particular redox potential that is conferred by their specific environment:<sup>10</sup> while the heme  $b_L$  and  $b_H$  have a redox potential of -90 mV and 50 mV, respectively, the heme  $c_1$  has redox of 230 mV.<sup>20</sup> These specificities will allow us to selectively change the reduction state of certain hemes, which in turn brings a clear distinction between the photo-induced mechanisms of each heme-type.

## Material and methods

**The laser:** The 800-nm output of a 1 kHz regenerative amplifier is used to pump a home-made visible non-collinear optical parametric amplifier (NOPA, see ref.<sup>21</sup> for a detailed description) producing the 523-nm pump pulses with a full-width-half-maximum of 8 nm and a time duration of ~50 fs. A small fraction of the regenerative amplifier output is focused onto a 5-mm thick  $CaF_2$  crystal to provide a wide visible probe.

The pump and probe pulses are focused into spots of ~80 and ~55  $\mu\text{m}$  in diameter, respectively, at the sample position by means of reflective optics in order to avoid degradation of the instrument response function. The resulting pump-probe cross-correlation is about 150 fs. The polarization of the pump and probe beam are set at the magic angle. After passing through the sample, the probe beam is focused onto the 160- $\mu\text{m}$  input slit of the Triax 190 spectrometer, while using a 300 grooves/mm, 550-nm blaze wavelength grating and focused onto a 1024 pixel CMOS array. Such conformation allows for a probing window from 340 to 750 nm with a spectral resolution of 2.5 nm.

**Sample handling:** As an alternative to the common spinning cell with its moving parts and to the peristaltic pumping that necessitates large sample volumes, we use a home-made closed-loop flow-cell that requires a total sample volume of only ~250  $\mu\text{L}$ ,<sup>22</sup> a volume therefore comparable to that of the spinning cell with the advantage of having a steady window at the laser focus. The flow is generated by a turbisc micro-pump from the Swiss Center for Electronics and Microtechnology (CSEM)<sup>23</sup> and bubbles are removed from the circuit via a decantation chamber. The pump and probe pulses are focused onto a square quartz silica capillary of 0.5-mm path-length and 0.1-mm thick window. While connected to both, the decantation chamber and the capillary, the pump was generating a flow of ~0.1 mL/s that was sufficient to refresh the sample for each laser shot at 1 kHz repetition rate. Due to the small amount of sample, the oxidation state of the hemes as well as the possible degradation of the complexes was verified by recording their steady-state absorption using the probe beam. Each absorption spectrum consisted of an average of 40 consecutive images while flowing the solution. Note that by passing through the capillary, the probe beam contains an additional broad and featureless scattering signal. Consequently any adjustments of the beam path will confer each spectrum with a small, but specific background as shown in Figure 2 while comparing the red and green curves.

**The  $bc_1$  complexes:** The sample is prepared as described in.<sup>24</sup> Corresponding to a differential (reduced – oxidized) *c*-heme absorption of ~0.16 OD for the  $\alpha$ -band trough the 0.5-mm path length capillary (Figure 2) and assuming the differential extinction coefficient of  $18.8 \text{ mM}^{-1}\text{cm}^{-1}$ ,<sup>25</sup> the concentration of  $bc_1$  monomer was about 170  $\mu\text{M}$ . The fluence of the excitation pulses was kept low in order to avoid multiple excitation of a single complex. From the comparison between the  $c_1$ - and *b*-heme contribution to the steady state absorption and to the transient signal (as discussed later, Figure 8 A and B), only ~5% and ~3 % of the reduced  $c_1$ - and *b*-heme, respectively, are involved in the major ps-long signal. The absorption of the reduced *c*-heme band was virtually identical before (addition of dithionite) and after the experiment (after oxidation of the *b*-hemes), which confirms the stability of the complexes over the course of the experiment.

**Data treatment:** Since the probe pulses are temporally chirped by some hundreds of fs, a Group Velocity Dispersion (GVD) correction is performed in post data acquisition analysis. From the corrected data, several kinetics are extracted at wavelengths corresponding to the major transient features. This set of kinetic traces is globally fitted as a sum of exponential decays. The same exponential components are then used to fit the Eigenkinetics that results from a Singular Value Decomposition (SVD) of the data-set.<sup>26</sup> Along with the Eigen-spectra, the corresponding Decay Associated Spectra (DAS) are generated, which will be presented later.

## Results

Due to its low redox potential, the addition of dithionite to the *cyt bc<sub>1</sub>* solution, effectively reduces all the *c*-hemes while, in our preparation, it only reduces about 70% of the *b*-hemes as shown in Figure 2. Note that in dilute samples, dithionite effectively reduces all hemes. This estimate results from the fit of the absorption spectrum, described later (Figure 8 A). This partial reduction of the *b*-hemes is attributed to the presence of oxygen in solution as well as the high protein concentration (~170  $\mu$ M of *cyt bc<sub>1</sub>* monomer; see SI for calculations). Partial reduction of the *b*-heme pool could raise questions concerning the presence of different reduction states of the *bc<sub>1</sub>* complex (1, 2, 3 or 4 reduced *b*-heme per dimer). Indeed, the reduction state of one heme affects its local environment<sup>27</sup> and could influence other nearby hemes as in the case of the tightly packed chlorophylls within the photosynthetic reaction centers.<sup>28</sup>

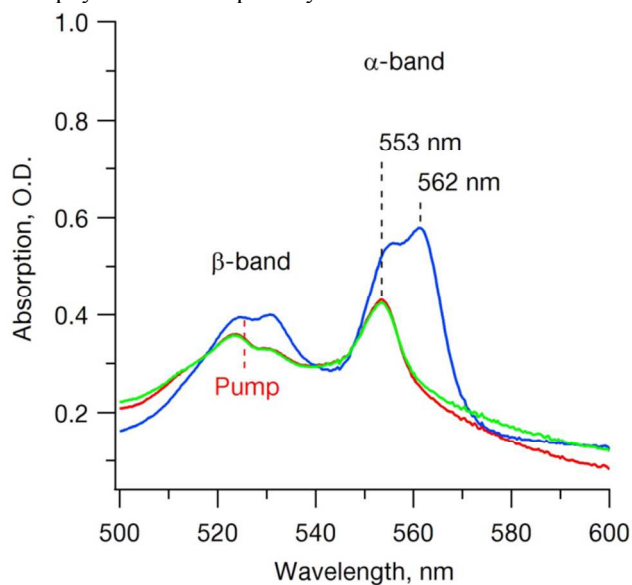


Figure 2: Static absorption spectrum of the sequential reduction and oxidation of the *cyt bc<sub>1</sub>* dimer complex: at the beginning of the experiment, after pre-reduction by ubiquinol and before (red) and right after (blue) the addition of dithionite, and at the end, after oxidation of the complexes by oxygen (green). The 523-nm excitation pump is indicated as reference.

It was however shown via Raman studies that heme *c<sub>1</sub>* is structurally isolated from the *b*-hemes, and that the local

environment of ferrous heme *b<sub>H</sub>* is unaffected by the redox state of heme *b<sub>L</sub>*.<sup>29</sup> Consequently we can assume that the partial reduction of the complexes, as opposed to a complete reduction, does not affect the individual behaviours of the hemes. The pump wavelength at 523 nm excites equally the  $\beta$ -band of both ferrous *b*- and *c<sub>1</sub>*-hemes. The resulting time-wavelength plot of the signal is shown in Figure 3 A. The response of both heme-types is seen by their respective bleach signals at 553 and 562 nm (horizontal dotted lines), as well as part of the mixed Soret-band signal from both heme *c<sub>1</sub>* and *b* at wavelengths < 470 nm. From the expected bi-phasic Soret-signal, as monitored for *cyt c*<sup>17,19</sup> and *cyt b<sub>5</sub>*,<sup>14</sup> only the positive lobe is observed. The resolution of the anticipated negative lobe is hindered due to the high optical density of the sample. Over the course of the experiment, the successive scans were marked by the oxidation of the *b*-hemes resulting in the loss of their corresponding signal at ~562 nm. Since the data do not show any long lived signal (>ns), we confirm that the oxidation of the *b*-hemes is not induced by the excitation pulses. If it were the case, we would expect the first scans to be characterized by a non-decaying transient signal representative of the photochemical processes leading to the oxidation of the *b*-hemes. The later oxidation is thus solely ascribed to the oxidative properties of dissolved oxygen molecules. Thus we take advantage of the properties of oxygen to fully oxidize the *b*-hemes while keeping intact the ferrous state of the *c<sub>1</sub>*-heme. The resulting transient signal (Figure 3 B) as well as the final absorption spectrum (Figure 2) shows clearly that only the 553-nm signal persists, corresponding solely to the ferrous *c<sub>1</sub>*-hemes. It is important to note that, while only the *c<sub>1</sub>*-hemes are reduced, the absence of a sharp feature around 562 nm confirms that the ferric state of the *b*-heme is unresponsive to light excitation and that the yield of photo-reduction, if any, is negligible while exciting the heme's  $\beta$ -bands (523 nm). Indeed, changes of the electronic state of the heme iron center are not expected while exciting above 400 nm.<sup>30</sup> It is also necessary to mention that further (post-experiment) addition of dithionite partially recovers the ferrous state of the *b*-hemes (data not shown), which proves that the *b*-hemes remains functional. The absorbance of the *c<sub>1</sub>*-heme  $\alpha$ -band remains virtually identical before and after the experiment, as shown in Figure 2; and the subsequent data analysis of the *c<sub>1</sub>*-heme alone gives, within the error margin of the fit, the same spectral features and exponential decay values prior to the first addition of dithionite and after full oxidation of the *b*-hemes by oxygen (as shown in SI). The temporal and spectral correspondence of the transient signal proves that the *c<sub>1</sub>*-hemes remain functional. We therefore conclude that neither dithionite, nor the presence of oxygen affects the protein complex and that its functionality remains intact in the course of the experiment.

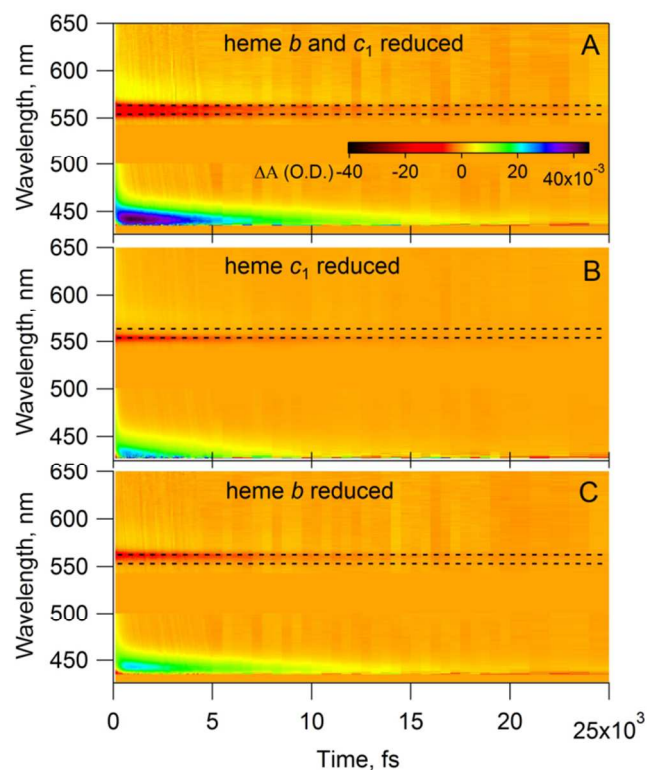


Figure 3: (A) Transient data taken right after addition of dithionite, while both  $b$ - and  $c_1$ -hemes are reduced. (B) Transient data taken after oxidation of the  $b$ -hemes by oxygen, while the  $c_1$ -hemes are left reduced. (C) Difference (A-B) corresponding solely to the signal of the ferrous  $b$ -heme, as discussed in text. The scattering region around the 523-nm excitation is set to zero. The horizontal dotted lines represent an eye-guide at 553 and 562 nm.

Since the selective oxidation of the  $b$ -hemes is done via solvated atmospheric oxygen molecules, the  $bc_1$  concentration remains identical before and after oxidation of the  $b$ -hemes and direct comparison of the two sets of data is therefore possible (Figure 3 A and B). This would not have been possible without some renormalization of the data, had we proceeded via successive reductions by adding solutions of ascorbate and then dithionite. Thus, the difference spectrum (A-B) corresponds to the signal associated with the ferrous  $b$ -hemes alone, as shown in Figure 3 C. One can see that the resulting data set (Figure 3 C) lacks any sharp features or any bleach signal that would be specific of the 553-nm band of the ferrous  $c_1$ -heme  $\alpha$ -band, which consequently, validates the data handling. To better illustrate the results of such a treatment of the data sets as well as the spectral evolution of each heme type we present in Figure 4 A, B and C, the transient spectra recorded at selected time delays, corresponding to the two-dimensional data of Figure 3 A, B and C, respectively. Note that we do not differentiate between hemes  $b_L$  and  $b_H$  since dithionite and oxygen are able to reduce and oxidize both, respectively. Moreover, even if heme  $b_L$  has a distinct split  $\alpha$ -band, it only appears as a shoulder at 554-nm in yeast  $bc_1$  complexes<sup>18</sup> with a differential extinction coefficient (reduced-oxidized) that is  $\sim 10$  times weaker compared to that of the combined 562-nm band of

both  $b$ -hemes. Since the present signal-to-noise ratio does not allow for the detection of such low signals, we refer to data set (B) and to the difference data set (C) in Figures 3 and 4 as representative of the overall  $c_1$ - and  $b$ -heme population, respectively.

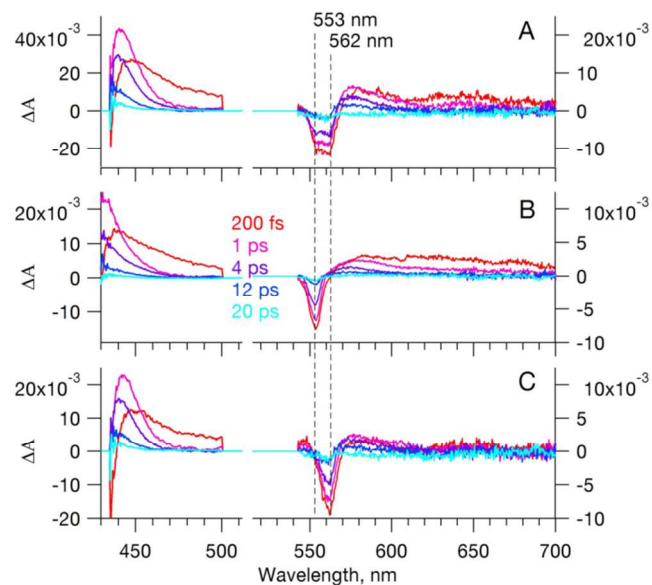


Figure 4: (A) Spectra at selected time delays while both  $b$ - and  $c_1$ -hemes are reduced. (B) Spectra at selected time delays while only the  $c_1$ -hemes are left reduced. (C) Difference (A-B) corresponding solely to the signal of the ferrous  $b$ -heme, as discussed in the text. Note that the vertical scales below and above 515 nm differs by a factor of two.

From these data sets, Figure 5 shows the globally fitted kinetic traces taken at selected wavelengths corresponding to the major spectral features. Satisfactory fits result in a minimum of three and two exponential decay components for the  $c_1$ - and  $b$ -hemes, respectively. The values of the decay constants used for the fits are given in Table 1. These exponential decay components agree with the components resulting from the Singular Value Decomposition (SVD) of the transient time-wavelength plots (Figure 3). The generated Decay Associated Difference Spectra (DADS) are presented in Figure 6. Because of the high protein concentration, the Soret band could not be monitored entirely. On the other hand, since the spectral changes in the  $\alpha$ -band region are better fingerprints of the redox and coordination state of the hemes, we will focus on the spectral region from 540 to 750 nm.

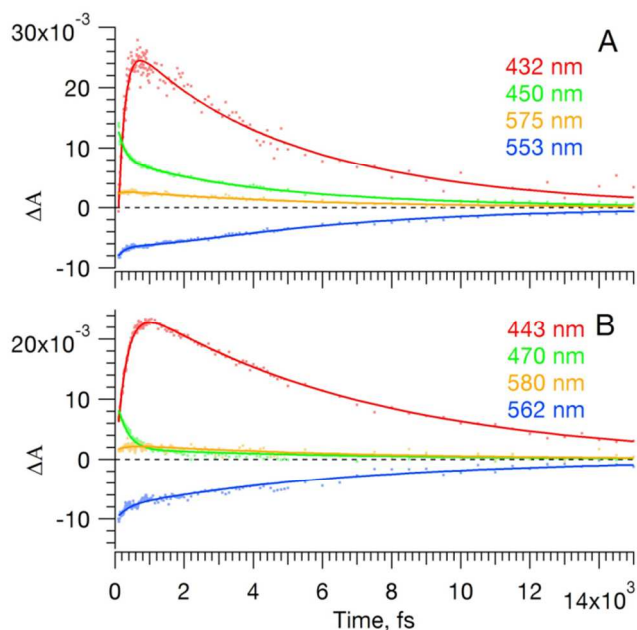


Figure 5: Kinetics traces of the hemes  $c_1$  (A) and  $b$  (B) respectively, at selected wavelengths and their global fit with a satisfactory minimum of three and two exponential decay components respectively.

**Table 1: Exponential decay components resulting from the global fit presented in Figure 5.**

	heme $c_1$	heme $b$
$\tau_1$	190 fs	300 fs
$\tau_2$	1.6 ps	-
$\tau_3$	5.4 ps	6.8 ps

## Discussion

**Heme  $c_1$ :** Because this work is the first ultrafast study on *cyt bc<sub>1</sub>*, we base our analysis of heme  $c_1$  in the *bc<sub>1</sub>* complex by comparing it with the *cyt c* whose heme and heme-environment are known to be structurally similar.<sup>13</sup> Because of their correspondence with the *cyt c* signals, the 190-fs is associated with an “intramolecular vibrational energy redistribution resulting in an equilibrated hot ground-state heme and possibly with a tail of the electronic relaxation”,<sup>31</sup> while the 1.6-ps components is mostly ascribed to an “intermolecular vibrational energy transfer from the hot heme to the surroundings”.<sup>31</sup> We would like to emphasize that these components cannot be representative of a single specific mechanism as the cooling processes are non-exponential.<sup>32, 33</sup> Indeed, both of these components show a broad positive amplitude to the red of the  $\alpha$ -band static absorption that is typical for the heme Excited State Absorption (ESA). It has been argued in the case of *cyt c* and met-myoglobin that this ESA partially stems from a pulse-limited electron and back

electron transfer between the porphyrin macrocycle to the  $d_z$  antibonding orbital of the iron.<sup>11, 15, 16</sup>

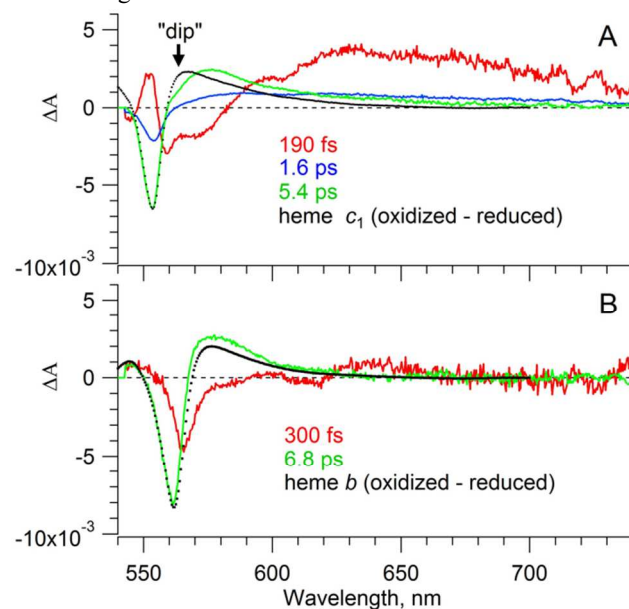


Figure 6: Decay Associated Difference Spectra of the  $\alpha$ -band spectral region corresponding to the  $c_1$ -hemes (A) and to the  $b$ -hemes (B). The oxidized minus reduced spectrum of each heme, normalized at the maximum bleach amplitude, is superimposed as reference only (black dotted line). The arrow points to a spectral feature that is specific of the photo-dissociated heme, as discussed in the text.

In the light of the subsequent  $b$ -heme spectral analysis, we can infer that part of the 540 to 580-nm region of the 190-fs DADS could also consist of a sharp Stimulated Emission (SE) similar to the 300-fs DADS component monitored for the  $b$ -heme (Figure 6 B). In order to differentiate the other concomitant processes from this expected SE, we subtract, from the  $c_1$ -heme's 190-fs DADS, the expected SE contribution by using the  $b$ -heme's 300-fs DADS that is blue-shifted by 9 nm (Figure 7, green curve). This shift is supposed to account for the difference in absorption and expected SE between the  $c_1$ - and  $b$ -hemes. Note that such straightforward subtraction is valid as long as the extinction coefficients, overall reactivity and emission Stokes-shift of both heme-types are similar. Variation of  $\pm 50\%$  in the subtracted SE amplitude however does not significantly affect the overall shape of the resulting difference spectrum. The blue curve in Figure 7, shows the resulting difference spectrum, which resembles that of the (reduced – oxidized) heme  $c_1$ , slightly red shifted by  $\sim 0.5$  nm. Because the band resembles that of the ferrous heme  $c_1$  and is positive, it corresponds to the formation of a 6-*c* reduced species (decrease of an initial bleach signal). The small shift also suggests that it is a hot state. The features above 560 nm are ascribed to a broad ESA signal (positive featureless band), that is decaying in 190 fs (decay of an initially positive signal). Similar short-lived ESA signal ( $\sim 500$  fs) have been reported for different myoglobin (Mb) samples and have been specifically assigned to the resulting charge transfer (CT) state (from the porphyrin ring

to its metal center) that triggers ligand dissociation.<sup>34, 35</sup> Correspondingly, we conclude that the short-lived broad ESA monitored for the heme  $c_1$  are also indicative of the heme's CT state.

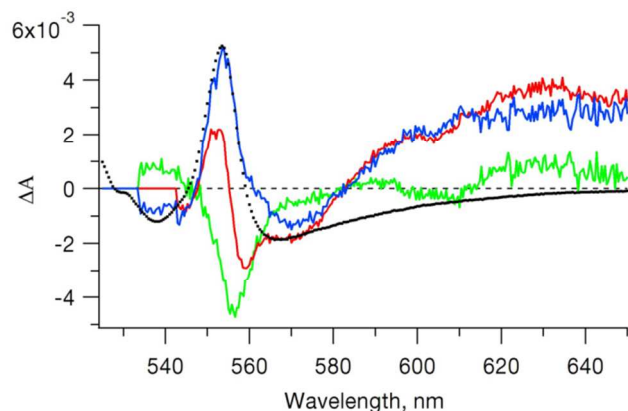


Figure 7 : The adjusted 300-fs Decay Associated Difference Spectra (DADS) of the *b*-heme signal (green) is subtracted from the 190-fs DADS of the  $c_1$ -hemes (red). The resulting difference spectrum (blue) is superimposed with the 5.4-ps DADS of the (reduced - oxidized) heme  $c_1$  (black dots) used for comparison only.

Since the SE, ESA and the formation of a 6-c ferrous *c*-heme are concomitant, we suggest that an initially excited *c*-heme, having lost its reduced 6-c character via an impulsive CT from the heme macrocycle to the metal center,<sup>16</sup> gives rise to the SE and ESA, and relaxes within 190 fs into its hot ground state through a non-dissociative pathway.

The bleach of the 1.6-ps DADS is slightly broader and red-shifted compared to the static  $c_1$ -heme  $\alpha$ -band. Since it is representative of the cooling of a hot 6-c species, it could be ascribed to the non-dissociative relaxation channel as proposed in the case of *cyt c*.<sup>15, 19</sup> Note that the 190-fs and 1.6-ps DADS only illustrate a mixture of the different non-exponential cooling mechanisms. Consequently, our assignment of particular processes to specific DADS features is approximative.

The 5.4-ps DADS, corresponding to the longest lived signal, is comparable to any transient spectrum taken after completion of the electronic and vibrational relaxation (from  $\sim 2$  to 10 ps). It is for example comparable to the different transient absorption spectra reported for *cyt c*.<sup>15, 19</sup> Following similar analysis, we can distinguish in the 5.4-ps DADS, the bleach of the *c*-heme  $\alpha$ -bands from the absorption spectrum of the photo-product, characterized by the broader ESA. While superimposed with the *c*-heme (oxidized - reduced) spectrum, as shown in Figure 6 A, the photo-product exhibits clearly a broad red-shifted absorption that extends beyond 700 nm. The same contrast is present in *cyt c* while comparing its oxidized spectrum (Figure 2 of ref.<sup>30</sup>) with the corresponding generated photo-product spectrum,<sup>19</sup> i.e. the *cyt c* photo-product's absorption spectrum is broader and red-shifted. Similarly, the *cyt c* photo-product represented in Figure 6 of ref.<sup>15</sup> shows exactly the same

features, including even the small "dip" at  $\sim 555$  nm. This "dip" is also present in our spectrum and is represented by the oxidized minus reduced heme *c* spectrum being above the 5.4-ps DADS near 560-565 nm (arrow in Figure 6 A). It was concluded that the generated *cyt c* photo-product corresponds to the photo-dissociated heme<sup>19</sup> based on the similarity of its transient signal with the 5-coordinated (5-c) MP-8 spectrum that is structurally analogous to the 5-c *cyt c*. Assuming that the broad and red-shifted spectrum, in respect to the oxidized species, along with the "dip" on the red-side of the  $\alpha$ -band are signatures of the 5-c photo-product, we conclude that the  $c_1$ -hemes in the  $bc_1$  complex also undergo photo-dissociation of one of their axial ligand.

The life time matches the 5-7 ps reported for the photo-cycle of a variety of 6-c hemes proteins, including *cyt c*.<sup>11, 15, 17, 19</sup> All these reports are unanimous in assigning this time constant to the rebinding of the photo-dissociated ligand. It should be mentioned that the 5.4-ps DADS might not be entirely free from other processes as vibrational cooling has previously been monitored with a life-time of  $\sim 4.6$  ps.<sup>36</sup> However, since the position and width of the transient bleach is identical to that of the static  $\alpha$ -band absorption, any contribution to the 5.4-ps DADS from vibrational cooling has to be minimal. Based on the correspondence of the overall monitored spectral features and life times with the literature, we conclude that the 5.4-ps component most probably corresponds to the rebinding of the photo-dissociated heme. As in *cyt c*, we suggest the dissociation of the Met residue.<sup>15, 37</sup>

**Heme *b*:** The corresponding data set could be satisfactorily fitted with only two exponential decays, which points to the fact that cooling dynamics differ from those monitored for the  $c_1$ -hemes. The 300-fs DADS is in fact singular as it does not show any significant positive signal expected from the ESA. It is however characterized by a sharp bleach to the red of the  $\alpha$ -band, and is of similar width. This feature is particular to the expected SE from the excited  $\alpha$ -band of the 6-c ferrous heme, therefore associated to a non-dissociative relaxation pathway. The absence of ESA signal in the *b*-heme's 300-fs DADS indicates that CT states, similar to the ones discussed in the case of the hemes  $c_1$ , are not generated. Consequently we do not expect the axial ligands of the *b*-hemes to dissociate.

The absence of a component similar to the 1.6 ps monitored for the heme  $c_1$  as well as for *cyt c* indicates that the relaxation of the excited *b*-hemes, which do not contribute to the longer 6.8-ps signal, occurs mainly within the first 300 fs. This ultrafast relaxation to the ground state has to be conferred to the *b*-heme from its environment.

As a matter of fact, the longer 6.8-ps DADS component (Figure 6 B) compares remarkably well to the oxidized minus reduced static spectrum of the *b*-hemes (ascorbate - dithionite). The small extra positive  $\sim 580$ -nm signal present in the 6.8-ps DADS might probably result from a small fraction of hot photo-product with corresponding cooling life-time. However since the width and bleach position are identical and we can expect that vibrational cooling, if any, has a negligible

contribution in the 6.8-ps DADS. The spectral features of the positive red-wing differ from that of the previous  $c_1$ -heme (5.4-ps DADS of Figure 6 A); namely, a shifted red-wing, while compared to its corresponding oxidized minus reduced static spectrum; a broad positive ESA signal that extends beyond 700 nm; and the “dip” to the red of the alpha band. By assuming that these “discrepancies” are a signature of the 5-c state of the hemes, their absence in the 6.8-ps DADS are also indicative that the  $b$ -heme behaves differently compared to the  $c_1$ -heme, and most probably does not photo-dissociate with its axial ligand. Together with its particular spectral features that mimic the oxidized minus reduced spectrum, we propose that the  $b$ -hemes undergo photo-oxidation. Photo-oxidation in cyt is well-known but typically implies the formation of a photo-induced electron acceptor. For example the tetra-heme cytochrome (THC) oxidizes as a result of the light-induced oxidation of nearby reaction centers.<sup>38</sup> Similarly, the cyt P450-BM3 oxidizes after photo-excitation of its covalently attached ruthenium complex.<sup>39</sup> The suggested  $b$ -heme’s photo-oxidation differs as it results from direct excitation of the heme. In this respect, photo-oxidation by means of visible-light excitation is unusual among cyt’s<sup>30</sup> and it requires further evaluation.

The different binding environments of the  $c_1$ - and  $b$ -hemes (Figure 1) may explain their different behaviours, because these environmental differences confer to each heme a particular spectrum and redox potential.<sup>9, 10</sup> Cyt  $b_5$ , structurally homologous to the  $b$ -hemes in cyt  $bc_1$ ,<sup>13</sup> is known to behave similarly to cyt  $c$ <sup>30</sup>. However the difference in Raman signal between the cyt  $b_5$  and the  $b$ -hemes in cyt  $bc_1$ <sup>13</sup> shows that we can also expect a different behavior for the  $b$ -heme with respect to cyt  $b_5$  and cyt  $c$ . Hereafter, we present different arguments supporting the possibility of photo-oxidation of the  $b$ -hemes in cyt  $bc_1$ :

- (1) Stronger physical constraints are exerted by the protein backbone onto the  $b$ -heme, resulting in the loss of planarity of the  $b_L$  heme.<sup>40</sup> The higher protein constraint that is exerted on the hemes certainly stiffens the His-heme-His ligation and impedes the possible dissociation of these axial ligands. Since photo-dissociation is hindered, other processes are expected to prevail.
- (2) Similar photo-oxidation reactions have been reported for both cyt  $c$  and cyt  $b_5$ , however, with excitation above 400-nm and the yield was judged negligible.<sup>30</sup> The same study shows however that the photo-oxidation cross section of cyt  $b_5$  is about 18 times higher than that of cyt  $c$  which, by analogy, shows that the  $b$ -heme is much more prone to photo-oxidation than the  $c_1$ -heme.
- (3) Photo-oxidation mechanisms were previously used to interpret signals from the 6-c heme-based oxygen sensor Dos excited with a  $\sim$ 30-fs, 563-nm low energy pulse,<sup>41</sup> therefore similar to our  $\sim$ 50-fs, 523-nm pulse. The corresponding signals were long-lived ( $>$ ns) and contributed only to 4-8 % but, keeping in mind that the protein complexes are different, this study indicates that photo-oxidation is feasible while exciting the heme Q-bands.
- (4) The photo-oxidation properties of the THC are commonly used in light-induced electron transfer reactions.<sup>38, 42</sup> The transient study of these THCs are however limited to the micro-seconds to minutes time range. Nevertheless, we note that the photo-oxidation reactions involve primarily the THC’s low potential  $c$ -type hemes that have redox properties corresponding to those of the  $b$ -hemes in the  $bc_1$  complex.
- (5) Interestingly, it was shown that oxidation of the  $b$ -heme by oxygen in cyt  $bc_1$  happens without the need of a ligand dissociation.<sup>43</sup> It consequently presupposes that the electron transfer occurs via molecular intermediates rather than by direct contact with the iron center that would necessitate dissociation of the His ligand. Our results indeed coincide with the fact that electron transfer can be readily initiated from the  $b$ -heme without the need for close contact with an external electron acceptor such as quinones or molecular oxygen.
- (6) It was also reported that the axial histidylimidazole ligands of the  $b_L$  heme has a distinct ionic character,<sup>40</sup> which would favour electron transfer processes. This electronegative character of at least one of the two His ligands was explained by the presence of nearby arginine residues.
- (7) When compared to the compilation of the optimal rate-distances from Moser et al<sup>44</sup> we see that an electron tunnelling life-time of 6.8 ps would correspond to donor-acceptor distances smaller than 6 Å. Such short distances match with the His being the electron acceptor as it lies at an average minimal distance of 2.0 Å from the heme’s iron center (according to the crystallographic data, PDB-file 3CX5<sup>7</sup>).
- (8) Finally, it is known that His residues actively participate in charge transfer processes and more specifically it was demonstrated that they can serve as electron acceptors.<sup>45</sup>

In the light of these arguments, we infer that the 6.8-ps DADS corresponds to the photo-oxidation of the  $b$ -hemes. Furthermore we expect heme  $b_L$  to predominantly contribute to our signal with the His residue playing the role of the electron acceptor.

**Quantum yield:** The goal of this section is to evaluate the reactivity of each heme-type, i.e. the photo-dissociation and the photo-oxidation of the heme  $c_1$  and  $b$ , respectively. In order to do so, we deconvoluted both the initial absorption spectrum (after addition of dithionite, Figure 8A) and the 5.4-ps DADS (generated from the first data set after addition of dithionite, Figure 8B) in terms of the  $c_1$ - and  $b$ -hemes’s (reduced-oxidized) spectrum. From the comparison of each heme’s relative contributions to both spectra, we see that  $\sim$ 5 % and  $\sim$ 4 % of the  $c_1$ - and  $b$ -hemes, respectively, contributed to the signal as described in Table 2. Alternatively, deconvolution of the final absorption spectrum (after oxidation of the  $b$ -hemes, Figure 8C) gives the same  $c_1$ -hemes contribution as did the initial absorption spectrum (Figure 8A). The conservation of the  $c_1$ -heme’s absorption amplitude during the experiment proves that its ferrous state was not affected by oxygen. The

fitting results are given in Table 2, while the details of the fitting procedure and calculations are to be found in the SI. Considering the fit of Figure 8B, weighing the coefficients obtained for each heme type by its respective extinction coefficient, i.e. 18.8 and 28.5  $\text{mM}^{-1}\text{cm}^{-1}$  for the  $c_1$ - and  $b$ -hemes, respectively,<sup>25</sup> and taking into account that we can only expect signal from the  $\sim 70\%$  ferrous  $b$ -hemes, it results that the reactivity of the  $b$ -hemes is  $\sim 50\%$  that of the  $c$ -hemes (assuming that we are equally exciting both heme-types).

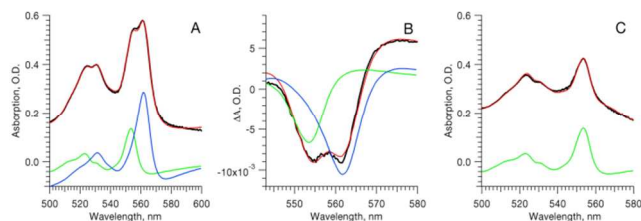


Figure 8: The black curves represent (A) the static absorption spectrum after addition of dithionite, (B) the DADS corresponding to the longest ps component resulting from the combined analysis of the  $b$ - and  $c_1$ -heme transient signals (see SI); while both are reduced and (C) the static absorption spectrum after full oxidation of the  $b$ -hemes via oxygen. Superimposed are the fits (red) and their components: the (reduced – oxidized) heme  $c_1$  (green) and heme  $b$  (blue) spectrum. The background-component used in each fit, not shown here for clarity, is described in SI.

**Table 2 : Amplitude of the heme  $c_1$  and  $b$  components resulting from the fitting of each plot in Figure 8.**

	Figure 8A	Figure 8B	Figure 8C
heme $c_1^*$	$A_{\text{heme } c} = 3.88$	$0.189 =$ $A_{\text{heme } c} \times 4.9\%$	3.93
heme $b^*$	$A_{\text{heme } b} = 2.8$	$0.103 =$ $A_{\text{heme } b} \times 3.7\%$	-

\* (reduced-oxidized) spectrum amplitude

If we assume that the photo-dissociation quantum yield of the  $c_1$ -heme in *cyt bc<sub>1</sub>* is comparable to the  $>0.8$  in *cyt c*<sup>19</sup>, because of their correspondence in structure, transient spectra and exponential decays, then the photo-oxidation quantum yield of the  $b$ -hemes is expected to exceed 0.4. This is to our knowledge, the highest reported photo-oxidation quantum yield for cytochromes, while the hemes are directly excited by visible light. The physiological consequences of such high reactivity are discussed subsequently.

**Mechanistic consequences:** The  $b$ -heme's high electronic reactivity makes perfect sense in the light of *cyt bc<sub>1</sub>* having to efficiently fulfil its role in the Q-cycle: in order to mediate the reduction and oxidization of the ubiquinone and ubiquinol, respectively. The  $b$ -hemes have to efficiently “process” the electrons, which demand them to easily lose or gain electron. Similar electronic-reactivity would in fact be counterproductive

in soluble cytochromes as they would less efficiently keep their electrons from being scavenged by other solutes. In purified reaction centers, it was in fact shown that the electron resulting from charge separation, while at the periphery of the complex could readily be “lost” to the solution.<sup>46-48</sup> The hydrophilic environment of the  $bc_1$  core on the other hand preserves the  $b$ -hemes from unwanted solvated electron carrier and their high electronic reactivity is then an advantage.

The fact that efficient electron migration is initiated via visible light also indicates that the protein might behave differently under dark and light conditions. We can further speculate that the overall catalytic efficiency of *cyt bc<sub>1</sub>* is light-dependent. We can then contemplate the protein complex as an active element in phototherapy for example.<sup>49</sup> It is also of interest to compare the light-responses of the  $bc_1$  complex with that of its photosynthetic homologue, the *cyt b<sub>6</sub>f*<sup>50</sup>. Being an essential component of the photosynthetic electron transport chain and being therefore exposed to direct sun-light, the foreseen specificity of the heme responses to light excitation could affect the photosynthetic's Q-cycle.

In contrast to the high electronic reactivity of the  $b$ -hemes, the high photo-dissociation quantum yield of the  $c_1$ -hemes can be understood as being an efficient “heat sink” that protects the reduced state of the heme against light excitations. The fact that the ferrous state of heme  $c_1$  is stable and protected implies the need for a change in local environment in order for the electron to proceed from heme  $c_1$  to the *cyt c*. Such conformational changes could readily be induced by the motions of the adjacent Rieske iron-sulfur complex.<sup>1</sup> Speculations put aside, it is remarkable that, even though the  $b$ -hemes in *cyt bc<sub>1</sub>* and in other *cyt b* have similar ligation to their protein backbone; specific structural constraints and amino-acid arrangements result in clearly different responses, and therefore functions. While cytochromes were known to serve only as electron carriers, this study demonstrates that with the appropriate environment, light-induced charge separation can readily be initiated within single heme structures. This singular behaviour consequently illustrates the importance of the local heme-bonding and structural environment in initiating larger chemical reactions.

## Conclusion

This study reveals the clear differences between the  $b$  and  $c_1$ -hemes behaviours within the  $bc_1$  protein complex: While the  $c_1$ -hemes undergo photo-dissociation of their axial ligand as a result of ultrafast laser excitation, the  $b$ -hemes most likely undergo photo-oxidation with a high ( $> 0.4$ ) quantum yield that is beyond all expectations. The recombination of the photo-dissociated ligand with the  $c_1$ -heme occurs in 5.4 ps, which is comparable to the value reported for a large range of cytochromes.<sup>17</sup> The efficient photo-oxidation of the  $b$ -heme is presumably linked to the stronger physical constraints exerted by the protein backbone onto the  $b$ -heme.<sup>40</sup> We suggest that these constraints hinder the flexibility of the adjacent His residues, and along with the induced ionic character of these

same His ligand,<sup>40</sup> favor the electron transfer process. The subsequent charge recombination takes place in 6.8 ps, in agreement with our estimate of the electron residing on the axial His residue. It is to keep in mind that not all ferrous *c*<sub>1</sub>- and *b*-hemes take part in these photo-reactions, and that, while the remaining excited *c*<sub>1</sub>-hemes exhibit relaxation mechanisms that are mainly illustrated by broad ESA signals, the cooling-down of the remaining excited *b*-hemes do not show any significant ESA. Besides pointing to the fact that the *c*<sub>1</sub>- and *b*-hemes behave and therefore function differently, these spectral differences call for further studies such as time-resolved fluorescence measurements<sup>16</sup> in order to evaluate the nature of these non-dissociative and non-oxidizing pathways. We confirm that the ferric form of *b*-heme types in the *bc*<sub>1</sub> complex is electronically inert under our excitation regime, i.e. that it does not undergo photo-reduction to any discernable extent. Finally, the high efficiency of the heme photo-oxidation clearly illustrates the high electronic reactivity of the ferrous *b*-hemes, which can be linked to their high efficiency in mediating the catalysis of ubiquinones and ubiquinolins within the cell membrane.

### Acknowledgments

This project has been funded by the Swiss NSF via the NCCR: MUST and by the FP7 Marie Curie COFUND.

### Notes and references

<sup>a</sup>Ecole Polytechnique Fédérale de Lausanne (EPFL), Laboratoire de Spectroscopie Ultrarapide, ISIC, Faculté des Sciences de Base, Station 6, 1015 Lausanne, Switzerland.

<sup>b</sup>Albert-Ludwigs-Universität Freiburg, BIOSS Centre for Biological Signalling Studies, Institute for Biochemistry and Biology, Stefan-Meier-Str. 17, 79104 Freiburg, Germany.

\*Corresponding Author

Phone: (+41) 21-693-0457

E-mail: majed.chergui@epfl.ch

1. E. A. Berry, M. Guergova-Kuras, L. Huang and A. R. Crofts, *Annu. Rev. Biochem.*, 2000, **69**, 1005-1075.
2. A. R. Crofts, *Biochem. Biophys. Acta*, 2004, **1655**, 77-92.
3. B. L. Trumpower, *Microbiol. Rev.*, 1990, **54**, 101-129.
4. C. Hunte, S. R. N. Solmaz, H. Palsdóttir and T. Wenz, *Results. Probl. Cell Differ.*, 2007, **45**, 253-278.
5. C. Lange and C. Hunte, *PNAS*, 2002, **99**, 2800-2805.
6. R. Pietras, M. Sarewicz and A. Osyczka, *J. Phys. Chem. B*, 2014, **118**, 6634-6643.
7. S. R. N. Solmaz and C. Hunte, *J. Biol. Chem.*, 2008, **283**, 17542-17549.
8. F. A. Walker, *Chem. Rev.*, 2004, **104**, 589-615.
9. S. E. J. Bowman and K. L. Bren, *Nat. Prod. Rep.*, 2008, **25**, 1118-1130.
10. W. A. Cramer and D. B. Knaff, *Energy Transduction in Biological Membranes, a Textbook of Bioenergetics*, Springer-Verlag, New York, 1990.
11. C. Consani, G. Auböck, O. Bräm, F. van Mourik and M. Chergui, *Journal of chemical physics*, 2014, **140**, 025103.
12. M. Chergui, in *Comprehensive Biophysics*, ed. E. H. Egelman, Oxford: Academic Press, 2012, vol. 1, pp. 398-424.
13. D. D. Hobbs, A. Kriauciunas, S. Giiner, D. B. Knaff and M. R. Ondrias, *Biochem. Biophys. Acta*, 1990, **1018**, 47-54.
14. K. A. Jongeward, D. Magde, D. J. Taube and T. G. Traylor, *J. Biol. Chem.*, 1988, **263**, 6027-6030.
15. C. Consani, O. Bräm, F. van Mourik, A. Cannizzo and M. Chergui, *Chem. Phys.*, 2012, **396**, 108-115.
16. O. Bräm, C. Consani, A. Cannizzo and M. Chergui, *J. Phys. Chem. B*, 2011, **115**, 13723-13730.
17. M. H. Vos, A. Battistoni, C. Lechavue, M. C. Marden, L. Kiger, A. Desbois, E. Pilet, E. de Rosny and U. Liebl, *Biochemistry*, 2008, **47**, 5718-5723.
18. J. N. Siedow, S. Power, F. F. de la Rosa and G. Palmer, *J. Biol. Chem.*, 1978, **253**, 2392-2399.
19. W. Wang, X. Ye, A. A. Demidov, F. Rosca, T. Sjodin, W. X. Cao, M. Sheeran and P. M. Champion, *J. Phys. Chem. B*, 2000, **104**, 10789-10801.
20. C.-A. Yu, L. Yu and D. Xia, in *Encyclopedia of Biophysics*, ed. G. C. K. Roberts, Springer & European Biophysical Societies' Association, 2013, pp. 2679-2684.
21. C. Consani, M. Prémont-Schwarz, A. ElNahhas, C. Bressler, F. van Mourik, A. Cannizzo and M. Chergui, *Angew. Chem.*, 2009, **121**, 7320-7323.
22. A. Chauvet, T. Tibiletti, S. Caffarri and M. Chergui, *Rev. Sci. Instrum.*, 2014, **85**, 103118.
23. A. Lisibach, E. Casartelli and N. Schmid, ASME 2010 3rd Joint US-European Fluids Engineering Summer Meeting and 8th International Conference on Nanochannels, Microchannels, and Minichannels, Montreal, Quebec, Canada, 2010.
24. T. Wenz, P. Hellwig, F. MacMillan, B. Meunier and C. Hunte, *Biochemistry*, 2006, **45**, 9042-9045.
25. W. H. Vanneste, *Biochem. Biophys. Acta*, 1966, **113**, 175-178.
26. J. Helbing, L. Bonacina, R. Pietri, J. Bredenbeck, P. Hamm, F. van Mourik, F. Chaussard, A. Gonzalez-Gonzalez, M. Chergui, C. Ramos-Alvarez, C. Ruiz and J. López-Garriga, *Biophys. J.*, 2004, **87**, 1881-1891.
27. J. S. Valentine, R. P. Sheridan, L. C. Allen and P. C. Kahn, *PNAS*, 1979, **76**, 1009-1013.
28. A. Chauvet, J. Sarrou, S. Lin, S. P. Romberger, J. H. Golbeck, S. Savikhin and K. E. Redding, *Photosynth. Res.*, 2013, **116**, 1-9.
29. F. Gao, H. Qin, M. C. Simpson, J. A. Shelnut, D. B. Knaff and M. R. Ondrias, *Biochemistry*, 1996, **35**, 12812-12819.
30. Y. Gu, P. Li, J. T. Sage and P. M. Champion, *J. Am. Chem. Soc.*, 1993, **115**, 4993-5004.
31. M. Negrierie, S. Cianetti, M. H. Vos, J.-L. Martin and S. G. Kruglik, *J. Phys. Chem. B*, 2006, **110**, 12766-12781.
32. E. R. Henry, W. A. Eaton and R. M. Hochstrasser, *proc. Nat. Acad. Sci. USA*, 1986, **83**, 8982-8986.
33. P. Li and P. M. Champion, *Biophys. J.*, 1994, **66**, 430-436.

34. S. Ishizaka, T. Wada and N. Kitamura, *Photochem. Photobiol. Sci.*, 2009, **8**, 562-566.
35. J. W. Petrich, C. Poyart and J. L. Martin, *Biochemistry*, 1988, **27**, 4049-4060.
36. D. Löwenich, K. Kleineremanns, V. Karunakaran and S. A. Kovalenko, *Photochem. Photobiol.*, 2008, **84**, 193-201.
37. S. Cianetti, M. Nègreerie, M. H. Vos, J.-L. Martin and S. G. Kruglik, *J. Am. Chem. Soc.*, 2004, **126**, 13932-13933.
38. M. Yoshida, S. K. and K. Matsuura, *Plant and cell Physiol.*, 1999, **40**, 192-197.
39. M. E. Ener, Y.-T. Lee, J. R. Winkler, H. B. Gray and L. Cheruzel, *PNAS*, 2010, **107**, 18783-18786.
40. C. Le Moigne, B. Schoepp, S. Othman, A. Verméglio and A. Desbois, *Biochemistry*, 1999, **38**, 1066-1076.
41. U. Liebl, L. Bouzhir-Sima, L. Kiger, M. C. Marden, Lambry, J.-C., M. Nègreerie and M. H. Vos, *Biochemistry*, 2003, **42**, 6527-6535.
42. D. Garcia, P. Richaud, J. Breton and A. Verméglio, *Biochimie*, 1994, **76**, 666-673.
43. L. Kiger, L. Tilleman, E. Geuens, D. Hoogewijs, C. Lechauve, L. Moens, S. Dewilde and M. C. Marden, *PLoS ONE*, 2011, **6**, e20478.
44. C. C. Moser, J. M. Keske, K. Warnck, R. S. Farid and P. L. Dutton, *Nature*, 1992, **355**, 796-802.
45. O. B. Morozova and A. V. Yurkovskaya, *Angew. Chem. internat. Edit.*, 2010, **49**, 7996-7999.
46. A. Chauvet, N. Dashdorj, J. H. Golbeck, T. W. Johnson and S. Savikhin, *J. Phys. Chem. B*, 2012, **116**, 3380-3386.
47. S. Savikhin, W. Xu, P. Martinsson, P. R. Chitnis and W. S. Struve, *Biochemistry*, 2001, **40**, 9282-9290.
48. A. Diaz-Quintana, W. Liebl, H. Bottin and P. Setif, *Biochemistry*, 1998, **37**, 3429-3439.
49. R. S. Dawe, *Brit. J. Dermatol.*, 2003, **148**, 626-637.
50. M. Schütz, M. Brugna, E. Lebrun, F. Baymann, R. Huber, K.-O. Stetter, G. Hauska, R. Toci, D. Lemesle-Meunier, P. Tron, C. Christian Schmidt and W. Nitschke, *J. Mol. Biol.*, 2000, **300**, 663-675.